Indian Journal of Pure & Applied Physics
Vol. 64, November 2026, pp. 1251-1258
DOI: 10.56042/ijpap.v64i11.33881

# Performance Optimization of Lead-Free Cesium Tin Germanium Triiodide Perovskite Solar Cell

Divya Sharma[a*], Sachin Jain[b], Asisa Kumar Panigrahy[c], Seema Garg[a] & Mayuri Kulshreshtha[d]

[a]Department of Electronics and Communication Engineering, Ajay Kumar Garg Engineering College, Ghaziabad 201 015, India

[b]Department of Computer Science and Engineering, Ajay Kumar Garg Engineering College, Ghaziabad 201 015, India

[c]Department of Electronics and Communication Engineering, ICFAI Foundation for Higher Education, Hyderabad 501 203, India

[d]Department of Computer Science and Engineering, IMS Engineering College, Ghaziabad 201 015, India

*Received: 15th July 2026; accepted: 12th October 2026*

High photovoltaic efficiency and cost-effective fabrication have made perovskite solar cells (PSCs) promising next-generation photovoltaic (PV) devices. The absorber, transport layers (electron & hole) strongly affects PSC performance. This study uses titanium dioxide ($TiO_2$) as the ETL, lead-free Cesium Tin Germanium Triiodide ($CsSnGeI_3$) and $CH_3NH_3PbI_{3-x}Cl_x$ as absorber materials and NiO, CuO as HTLs using numerical simulations. A systematic analysis examines how perovskite thickness, acceptor concentration & interface defect density affects device behaviour. The proposed device TCO/$TiO_2$/$CsSnGeI_3$/NiO/back-contact device performed best, with a Voc of 1.18 V, Jsc of 26.496 mA/cm², FF of 83.55 percent & η (PCE) of 26.19 percent. The optimized lead-free $CsSnGeI_3$ device achieves a 4.04% higher PCE than the existing cell, highlighting the potential of $CsSnGeI_3$ as a high-efficiency and environmentally friendly active material for perovskite solar cells.

**Keywords:** $CsSnGeI_3$, NiO, $TiO_2$, Perovskite solar cells (PSCs), Power conversion efficiency

## 1 Introduction

PSCs represent a leading-edge photovoltaic (PV) technology, that offers high PCE, low fabrication costs & solution-processable production. Since the first PSC reached 3.8 percent PCE in 2009[1], advances in materials engineering and device architecture have increased certified efficiency to over 27 %[2]. Charge carrier recombination, interfacial defects, thermal instability, & environmental degradation limit PSC stability and commercialization[3-6].

The performance of PSCs is strongly influenced by: absorber, transport layer (electron & hole). Several ETL materials, including $TiO_2$, $SnO_2$, ZnO, fullerene ($C_{60}$), and PCBM, have been extensively studied for PSC applications[7-11]. $TiO_2$ is a popular ETL due to its wide bandgap, high optical transparency, energy-level alignment, chemical stability and efficient electron transport[12].

Photon capturing and generation of charges takes place in the absorber layer. Conventional lead-based perovskites, especially $CH_3NH_3PbI_{3-x}Cl_x$, have good optical and electrical characteristics[12]. However, lead toxicity concerns have spurred the search for greener alternatives. Cesium Tin Germanium Triiodide ($CsSnGeI_3$) is a promising lead-free perovskite material owing to its favorable bandgap, strong optical absorption, efficient carrier transport and enhanced chemical stability[13].

The HTL extracts photogenerated holes and prevents interfacial charge recombination. A variety of HTLs, including CuSCN, Spiro-OMeTAD, PTAA, PEDOT, CuI, CuO & NiO, have been investigated for PSC applications[14-23]. Among the inorganic HTLs, both CuO and NiO exhibit good thermal stability and hole transport characteristics. However, NiO possesses a wide bandgap, higher optical transparency, favorable valence-band alignment, and excellent chemical stability, enabling more efficient hole extraction & reduced interfacial recombination losses[24-25]. Therefore, NiO was selected as the HTL for the proposed device, while CuO was employed in the conventional device for comparison.

Although significant progress has been achieved in PSC research, comparative studies of conventional Pb-based & Pb-free PSC architectures with optimized transport layers remain limited. In particular, the combined effects of perovskite thickness, acceptor

*Corresponding author: E-mail: divya13jan@gmail.com

concentration & interface impurities on the performance of $CsSnGeI_3$-based solar cells have not been comprehensively explored. Therefore, this work presents a comparative numerical investigation of existing $TCO/TiO_2/CH_3NH_3PbI_{3-x}Cl_x/CuO$ device and a proposed lead-free $TCO/TiO_2/CsSnGeI_3/NiO/Au$ device exploiting the SCAPS-1D software. The role of absorber thickness, acceptor concentration & interface defect density is systematically analyzed to identify the optimum device configuration. Compared with the conventional device, the proposed architecture combines the environmentally friendly $CsSnGeI_3$ absorber with the NiO HTL, resulting in improved charge extraction, reduced interfacial recombination & enhanced device stability. Consequently, the optimized $TCO/TiO_2/CsSnGeI_3/NiO/Au$ device exhibits a PCE of 26.19 %, providing a 4.04 % more enhancement than the conventional $CH_3NH_3PbI_{3-x}Cl_x$ device. These findings highlight the promise of the proposed lead-free design for creating stable, efficient, & ecologically friendly PSCs.

## 2 Methods and Materials

### 2.1 Device Simulation Methodology

This paper presents the simulation results of $CsSnGeI_3$ PSC modeled using the simulator (SCAPS-1D). For this simulation, this is the proposed $TCO/TiO_2/CsSnGeI_3/NiO/Au$ device. A maximum efficiency of 26.19 percent was observed in solar cell using NiO as the HTL, according to the optimized simulations. Figure 1 (a) and (b) depicts the device structure and Fig. 1 (b) simulated schematic of $CsSnGeI_3$ cell. The numerical simulation is performed using Poisson equation and continuity equations through SCAPS-1D[24].

$$Dn\frac{\partial^2 n(x)}{\partial x^2}+\mu E_n(x)\frac{\partial n(x)}{\partial x}+G_n(x)-R_n(x)=0 \quad \ldots (1)$$

$$Dp\frac{\partial^2 p(x)}{\partial x^2}-\mu E_p(x)\frac{\partial p(x)}{\partial x}+G_p(x)-R_p(x)=0 \quad \ldots (2)$$

Equations 1 and 2 use the following symbols: E(x), D, and μ to represent electric field across absorber material, diffusion coefficient & Hole/electron transportation respectively. The electron concentration is represented by n(x), while the photogeneration rate is symbolized by Gp(x). Recombination of holes is represented by Rp(x). Applying the Poisson and Continuity equation allows one to ascertain a number of parameters of solar cells. The device parameters for respective layer of the $CsSnGeI_3$ cell is illustrated in Table 1.

The lead-free $CsSnGeI_3$ performance is significantly affected by defects in the device's structure. When it comes to controlling the number of defects in a solar cell, the mathematical expression for Shockley-Read-Hall (SRH) recombination model is;

$$R=\frac{\tau_{n,p}^{-1}(np-n_i^2)}{n+p+2n_i cosh(\frac{E_t-E_i}{kT})} \quad \ldots (3)$$

where

$\tau_{n,p}$ : electron and hole carrier lifetimes

*ni*: intrinsic carrier concentration

*n/p*: electron & hole concentrations

$n_i$: intrinsic charge carrier concentration

$E_i$: Intrinsic-state energy level

$E_t$: trap energy level (energy level associated with the defect state)

The positive & negative charge carriers' thermal velocities in all layers remain constant at $10^7$ cm/s.

$$\tau_{n,p}=\frac{1}{\sigma_{n,p}v_{th}N_t} \quad \ldots (4)$$

$\tau_{n,p}$ as given in Eq. 4 stands for the electron and hole relaxation times in motion. $N_t$ and $\sigma_{n,p}$ represent the density of defects & the carrier capture cross-

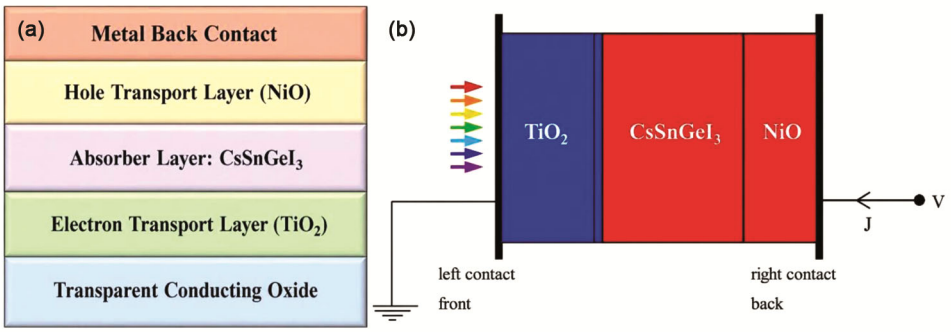


Fig. 1 — (a) Proposed $CsSnGeI_3$ device structure; and (b) Simulated $CsSnGeI_3$ device

Table 1 — Proposed PSC setting parameters for the design simulation

| Parameters | [12]TCO ($SnO_2$:F) | [12]ETM ($TiO_2$) | [13]Absorber Layer ($CsSnGeI_3$) | [15]HTM (NiO) |
|---|---|---|---|---|
| t (nm) | 500 | 50 | 650 | 400 |
| $E_g$ (eV) | 3.5 | 3.2 | 1.5 | 3.8 |
| EA (eV) | 4 | 3.9 | 3.9 | 1.4 |
| ε | 9 | 9 | 28 | 10.7 |
| $N_v$ (/cm$^3$) | $1.8\times10^{18}$ | $1.8\times10^{18}$ | $3.1\times10^{18}$ | $1.8\times10^{19}$ |
| $N_C$ (/cm$^3$) | $2.2\times10^{18}$ | $2.2\times10^{18}$ | $3.1\times10^{19}$ | $2\times10^{19}$ |
| $\mu_n$/ $\mu_p$ (cm$^2$/Vs) | 20/10 | 20/10 | 974/213 | 12/28 |
| $N_D$/$N_A$ (/cm$^3$) | $2\times10^{19}$ | $2\times10^{16}$ | $10^{14}$ | $10^{20}$ |
| $N_t$ (/cm$^3$) | $10^{15}$ | $10^{15}$ | $2.5\times10^{13}$ | $10^{14}$ |

section, respectively. The charge carrier diffusion length (L) is expressed as;

$$l = \sqrt{D\tau} \quad \text{... (5)}$$

In this case, D stands for the diffusion constant, which can be found by applying the given relation

$$\text{i.e. } D = \frac{\mu kT}{q} \quad \text{... (6)}$$

Various parameters were calculated using the aforementioned equations. The calculated values are in good agreement with the simulation results.

To estimate the light absorption coefficient (α), following equation is used;

$$\alpha = A_\alpha (hv - Eg)^{1/2} \quad \text{... (7)}$$

here $A_\alpha$ is $10^5$ cm$^{-1}$

## 3 Results and Discussion

To achieve optimal performance of $CsSnGeI_3$-based PSC, a systematic investigation was carried out by varying the absorber-layer thickness, acceptor concentration, & defect-state density. The effects of these parameters on the photovoltaic parameters i.e. Voc, Jsc, FF & $\eta$ *or* eta or PCE, are presented in the following subsections to determine the optimal device configuration.

### 3.1 Evaluation of the Most Appropriate HTL

As a whole, the photovoltaic performance of PSCs is improved by the HTL, which facilitates effective positive charge extraction & suppressing interface-mediated recombination. Figure 2 compares the performance of the proposed NiO HTL with the existing CuO HTL. The absorber thickness significantly affects device characteristics; increasing the layer thickness results enhanced optical absorption & charge carrier generation up to an optimum thickness, beyond which recombination losses increase, leading to a decline in PCE. The proposed $CsSnGeI_3$/NiO device exhibits optimum performance at an absorber thickness of 650 nm. The optimized simulation parameters listed in Table 1, while the respective photovoltaic results are presented in Table 2. Under identical HTL thickness conditions, the proposed lead-free $CsSnGeI_3$/NiO device achieves a Voc of 1.18 V, Jsc of 26.496 mA/cm², FF of 83.55 %, resulting in a PCE of 26.19 %, outperforming the existing $CH_3NH_3PbI_{3-x}Cl_x$ /CuO device. The outcomes highlight the potential of the proposed $CsSnGeI_3$ architecture for attaining superior performance and environmentally sustainable perovskite photovoltaic cells.

Based on these results, the optimum absorber thickness was adopted for all subsequent simulations.

### 3.2 Defect Density (Nt) Impacts on $CsSnGeI_3$ Layer

The resulting photovoltaic device characteristics of perovskite-based solar cells are greatly influenced by the defect density ($N_t$) of the $CsSnGeI_3$ perovskite layer, which strongly influences charge-carrier recombination and transport. Photovoltaic efficiency, open-circuit voltage, current density under short-circuit conditions, and fill factor are the outcomes of non-radiative recombination, which is facilitated by defect states that serve as trapping centres. Figure 3 shows how the photovoltaic parameters change with varying defect density. The study determined that $2.5 \times 10^{13}$ cm$^{-3}$ was the optimal value when the defect density was varied (i.e. in the range of $10^{13}$ & $10^{18}$ cm$^{-3}$). The carrier lifetime, recombination losses, and device stability are all negatively impacted by a rise in defect density because an increased number of trap states within the bandgap. These findings are consistent with previously reported results for

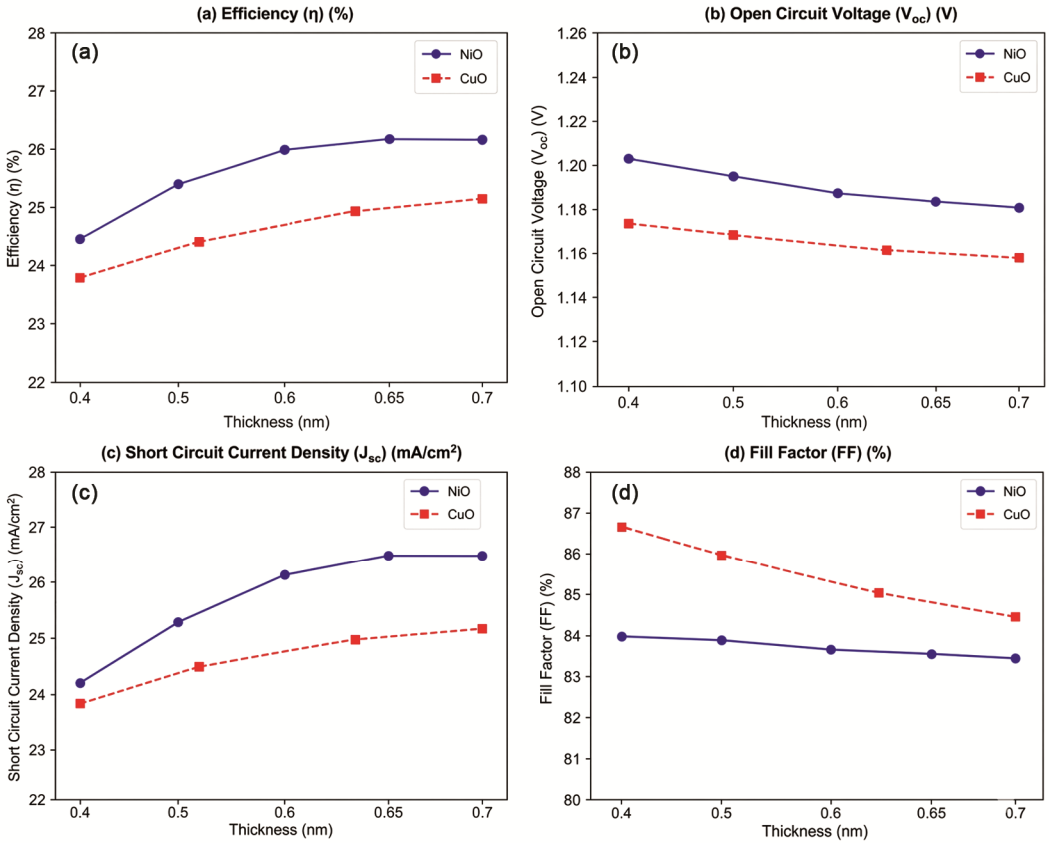


Fig. 2 — Variation of photovoltaic parameters with absorber thickness for the existing[2] and proposed PSC structures: (a) η (b) Voc (c) Jsc; and (d) FF

Table 2 — Evaluate the proposed cell in relation to the reference one

| Serial No. | Parameters | [12]Reference $CH_3NH_3PbI_{3-x}Cl_x$ Cell | Proposed $CsSnGeI_3$ Cell |
|---|---|---|---|
| i | $\eta$, PCE (%) | 25.172 | 26.19 |
| ii | FF (%) | 85.64 | 83.55 |
| iii | $V_{OC}$ (V) | 1.167 | 1.18 |
| iv | $J_{SC}$ (mA/cm$^2$) | 25.18 | 26.496 |

perovskite solar cells[26]. The proposed $CsSnGeI_3$/NiO device achieves the optimized photovoltaic performance in lead-free perovskite photovoltaic devices by attaining a Voc of 1.18 V, Jsc of 26.496 mA/cm², FF of 83.55 %, and PCE of 26.19 % at the optimal defect density.

### 3.3 Defect Density of $CsSnGeI_3$ Layer Impact on Recombination Rate

One way to describe the optoelectronic performance of the proposed $CsSnGeI_3$ device is to look at how the Shockley-Read-Hall (SRH) recombination model changes depending on the number of defects[27]. Improved device performance and longer charge carrier lifespan are the results of reduced defect density, which suppresses trap-assisted recombination. As illustrated in Fig. 4, the minimum recombination rate is observed at a defect density of $1 \times 10^{14}$ cm$^{-3}$. In contrast, increasing the defect concentration to $1 \times 10^{18}$ cm$^{-3}$ introduces additional trap states, significantly increasing the SRH recombination rate & consequently degrading the photovoltaic performance. The SRH recombination rate is expressed as follows[27];

$$R = \frac{\tau_{n,p}^{-1}(np - n_i^2)}{n + p + 2n_i cosh(\frac{E_t - E_i}{kT})} \quad \ldots (8)$$

In which,

$\tau_{n,p}$ - Carrier lifetime

$n$, $p$ -density of electrons and holes

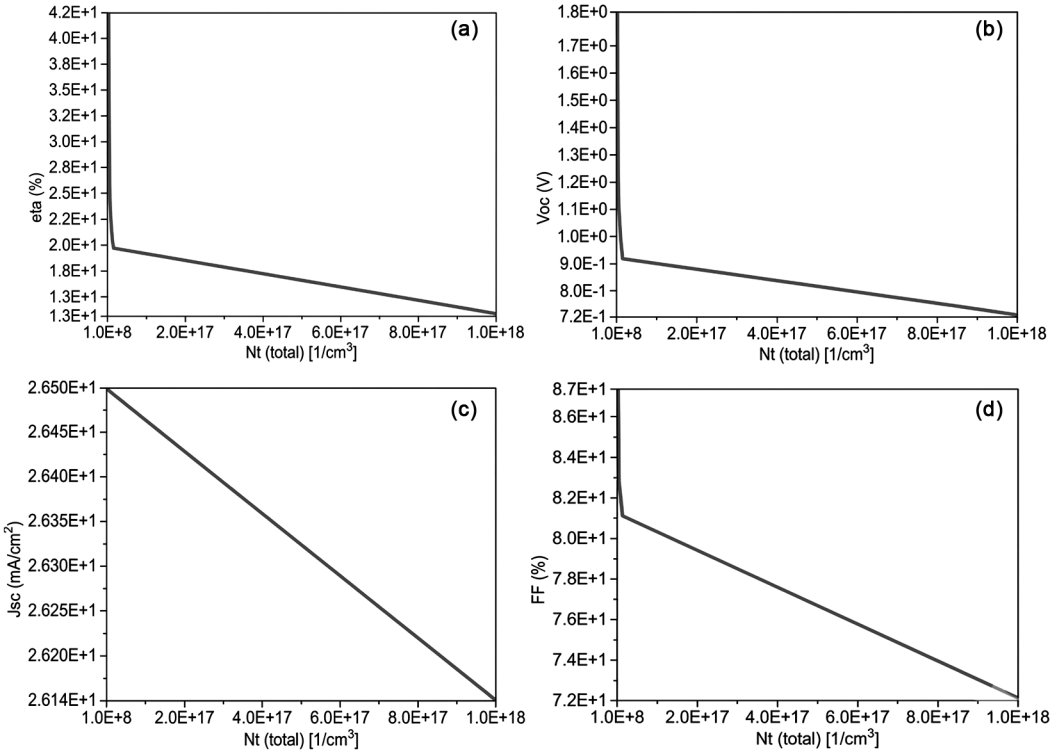


Fig. 3 — Total defect concentration of the $CsSnGeI_3$ layer correlates with cell properties: (a) η (b) Voc (c) Jsc; and (d) FF

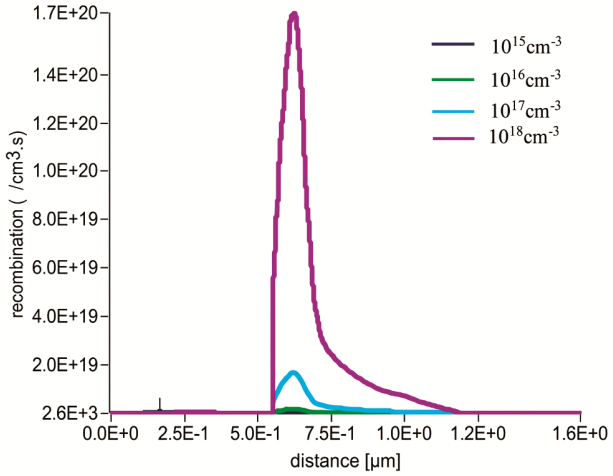


Fig. 4 — Variation of recombination rate with device depth at different defect concentrations

$n_i$, $E_i$ -internal energy and density

$E_t$ - Trap energy level

The average lifetime of electrons and holes before recombination;

$$\tau_{n,p} = \frac{1}{\sigma_{n,p} v_{th} N_t} \quad \ldots (9)$$

in which,

$\sigma_{n,p}$ -collected the electron and hole cross-sectional areas

$v_{th}$ -temperature at which electrons and holes move

$N_t$ - the density of defects in perovskites

The above equations indicate that increasing the defect density in the perovskite layer reduces lifetimes of carriers (the electron and hole), thereby increasing the Shockley-Read-Hall (SRH) recombination rate. Consequently, higher defect concentrations increase charge-carrier recombination, leading to deterioration in the photovoltaic device characteristics, as illustrated in Fig. 4. The carrier diffusion length ($L_D$) can be determined from the carrier lifetime using the following relation;

$$L_D = \sqrt{D\tau} \quad \ldots (10)$$

In this case, the diffusion coefficient is denoted by D. The concordance between the theoretical and simulated diffusion lengths provides strong evidence that the simulation model is accurate. The simulation also does not account for the impact of contact resistances, either series or shunt. The energy band arrangement of $CsSnGeI_3$-based PSC is illustrated in Fig. 5. Based on these results, the optimum defect density was employed in all subsequent simulations to maintain consistent conditions for subsequent simulations.

### 3.4 Influence of $CsSnGeI_3$ Layer Acceptor Concentration

A relationship between the photovoltaic performance of the designed PSC and the concentration of the acceptor is illustrated in Fig. 6. The device functions at its best when the concentration of the acceptor is $1 \times 10^{14}$ $cm^{-3}$. At the specified concentration, Voc, Jsc, and FF reached 1.18 V, 26.496 mA $cm^{-2}$, and 83.55 %, which is also the PCE. Raising the concentration of the acceptors improves the built-in electric field, leading to more efficient charge separation & less carrier recombination. Table 2 presents the corresponding photovoltaic parameters. Based on these findings, the optimum acceptor concentration was used the optimum acceptor concentration in all following simulations.

### 3.5 Quantum Efficiency Analysis

The EQE spectra of the optimized TCO/$TiO_2$ /$CsSnGeI_3$/NiO/Au solar cell are displayed in Fig. 7. Across the 300-600 nm wavelength range, the device displays an EQE above 90 %, suggesting excellent absorption of photons & collection of charge carriers. Due to decreased photon absorption and greater

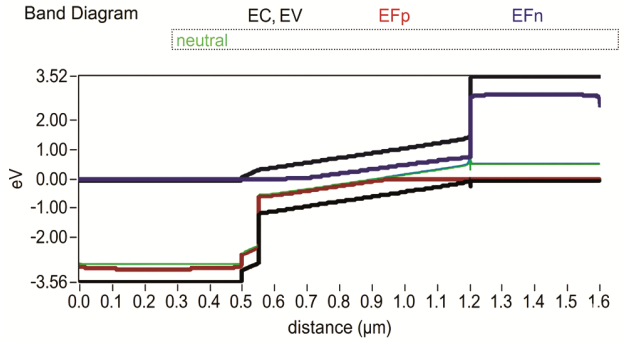


Fig. 5 — Energy band diagram of $CsSnGeI_3$ device

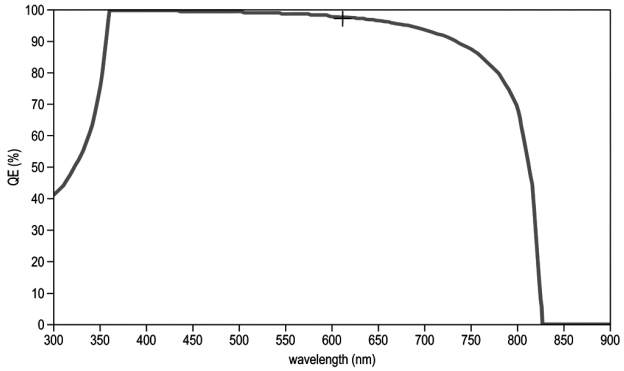


Fig. 7 — EQE spectra of the highly efficient PSC from the outside

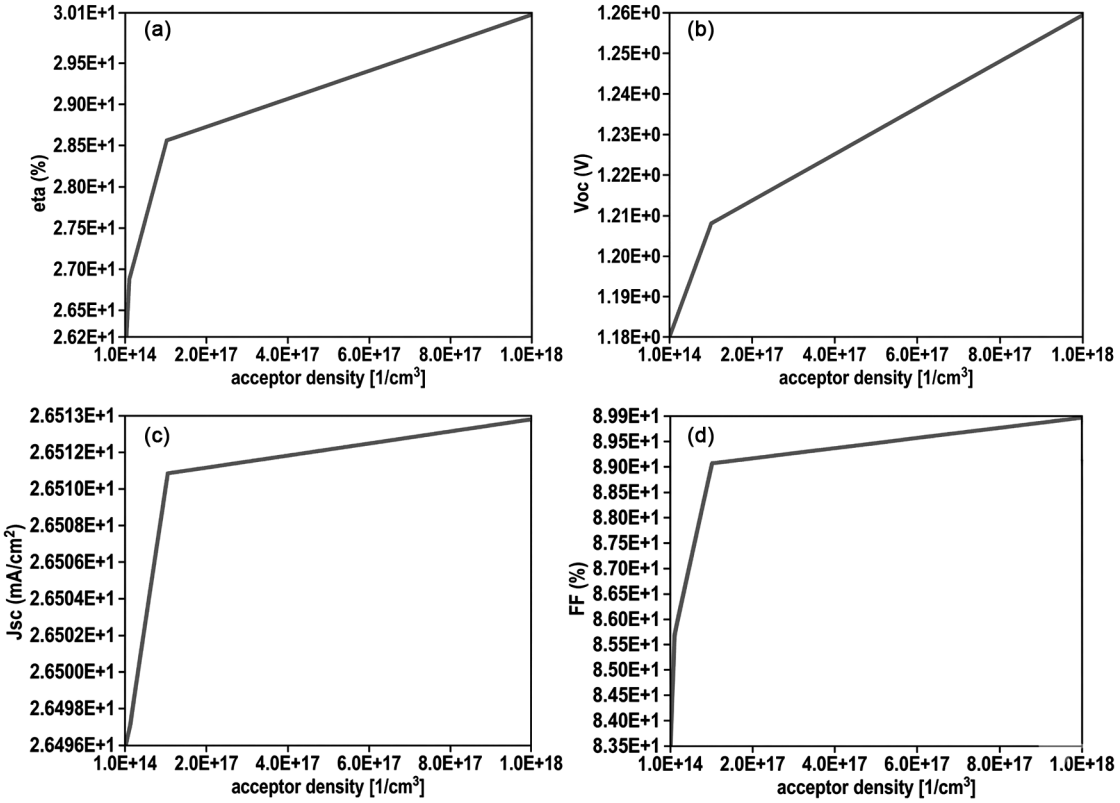


Fig. 6 — Photovoltaic parameter variation with respect to active layer donor density ($N_D$)**:** (a) η (b) Voc (c) Jsc; and (d) FF

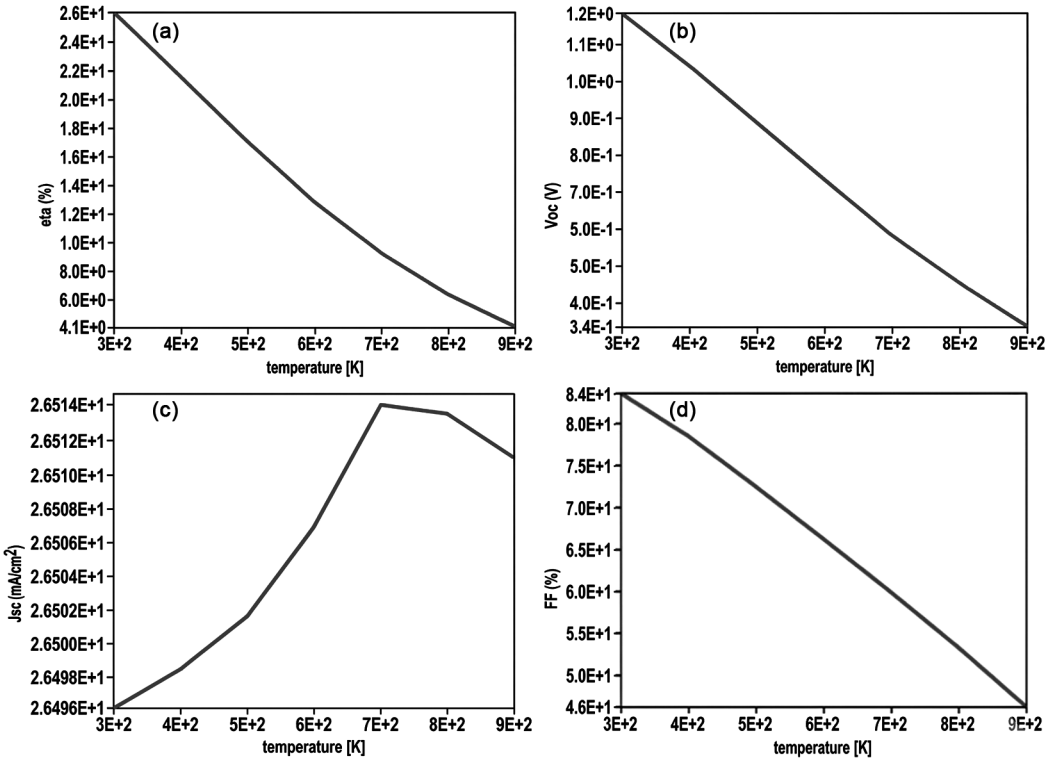


Fig. 8 — Effect of operating temperature on the photovoltaic parameters of the proposed PSC: (a) η (b) Voc (c) Jsc; and (d) FF

carrier recombination at longer wavelengths, the EQE gradually drops beyond this range. The optimised device's enhanced photovoltaic performance & short-circuit photocurrent density (Jsc) are consistent with the high EQE, confirming that the $TiO_2$/NiO transport layers are effective charge extractors.

### 3.6 Operating Temperature

The change in photovoltaic performance parameters of the proposed perovskite cell due to change in operating temperature has been demonstrated through Fig. 8. The efficiency (η), open-circuit voltage (Voc) & fill factor (FF) decrease significantly with increase in operating temperature from 300 to 900 K. However, short-circuit current density (Jsc) elevates till 700 K thereafter a marginal decrease in short-circuit photocurrent density (Jsc) has been observed at higher temperatures. The decrease in Voc and FF at higher temperatures results in overall decrease in perovskite solar cell performance[28-29].

## 4 Conclusion

A numerical comparison was performed between the conventional TCO/$TiO_2$/$CH_3NH_3PbI_{3-x}Cl_x$/CuO device and the proposed lead-free TCO/$TiO_2$/$CsSnGeI_3$/NiO/Au device. The optimized solar cell achieves a PCE of 26.19 %, along with an FF of 83.55 % and a Voc of 1.18 V, the proposed device outperformed the highest efficiency. The photovoltaic performance was systematically investigated by varying in terms of the absorber-layer thickness, acceptor density & defect density. The reduced recombination, effective charge extraction, and favourable energy-level alignment provided by the $CsSnGeI_3$/NiO combination contribute to the improved performance. In addition, the proposed lead-free design shows promise as an Eco-conscious and highly efficient perovskite photovoltaic device, with a PCE that is 4.04 percent higher than the conventional device. Experimental realization of the optimized device and evaluating its stability over the long period will be the primary goals of future research.

## References

1 Kojima A, Teshima K, Shirai Y & Miyasaka T, *J Am Chem Soc*, 131 (17) (2009) 6050.

2 National Renewable Energy Laboratory, *Best Research-Cell Efficiencies* (2026).

3 Baumann S, Eperon G E, Virtuani A, Jeangros Q, Kern D B, Barrit D, Schall J, Nie W, Oreski G, Khenkin M, Ulbrich C, Peibst R, Stein J S & Köntges M, *Energy Environ Sci*, 17 (20) (2024) 7566.

4 Baishya H, Adhikari R D, Patel M J, Yadav D, Sarmah T, Alam M, Kalita M & Krishnan Iyer P, *J Energy Chem*, 94 (2024) 217.
5 Yadav N & Khare A, *Surf Interfaces*, 56 (2025) 105593.
6 Elangovan N K, Kannadasan R, Beenarani B B, Alsharif M H, Kim M K & Inamul Z H, *Energy Rep*, 11 (2024) 1171.
7 Feng K, Wang G, Lian Q *et al.*, *Nat Mater*, 24 (2025) 770.
8 *Krishna B G, Ghosh D S & Tiwari S, Chem Inorg Mater, 1 (2023) 100026.*
9 *Sharma D, Mehra R & Raj B, J Semicond, 59 (12)* (2025) 1316.
10 Jia G, Fang Y, Song X *et al.*, *J Mater Sci*, 60 (2025) 7466.
11 Zang L, Zhao C, Hu X, Tao J, Chen S & Chu J, *Small*, 20 (2024) 2400807.
12 Thakur N & Mehra R, *J Nanoelectron Optoelectron*, 14 (2) (2019) 217.
13 Bhattarai S *et al.*, *Sustainability*, 15 (2023) 13955.
14 Dhakla S, Deendyal P K, Singh H, Mishra M, Kumar S & Kashyap M K, *Indian J Pure Appl Phys*, 61 (2023) 851.
15 Coulibaly A B, Oyedele S O, Kre N R & Aka B, *Model Numer Simul Mater Sci*, 9 (2019) 97.
16 Xu P, Lim E L & Wei Z, *ChemSusChem*, 18 (2025) e202500460.
17 Dixit K & Ahmad G, *Indian J Pure Appl Phys*, 62 (2024) 553.
18 Hossain M I, Alharbi F H & Tabet N, *Sol Energy*, 120 (2015) 370.
19 Sharma D, Mehra R & Raj B, *J Nano*, 21 (1) (2026) 2550021.
20 Tang Z, Yao D, Li Y, Li C, Xia T, Tian N, Wang J, Zheng G, Mo S, Long F & Zhou B, *ACS Appl Mater Interfaces*, 16 (18) (2024) 23973.
21 Lin Z, Zhang W, Cai Q, Xu X, Dong H, Mu C & Zhang J P, *Adv Sci*, 8 (22) (2021) 2102845.
22 Zhang W, Lin Z, Cai Q, Xu X, Dong H, Mu C & Zhang J P, *ChemSusChem*, 15 (3) (2021) e202102002.
23 Lin Z, Zhang W, Cai Q, Xu X, Dong H, Mu C & Zhang J P, *Sol RRL*, 6 (8) (2022) 2200343.
24 Wu Y, Xu L, Lv J, Du Y, Cai B, Wang R, Wang C & Zhang W-H, *Sol RRL*, 10 (2026) e202500789.
25 Karishma, Bamola P, Rawat S, Dangwal S, Dwivedi C & Sharma H, *Sol Energy*, 282 (2024)
26 Akshay V R, Arun B, Mandal G & Vasundhara M, *Phys Chem Chem Phys*, 21 (24) (2019) 12991.
27 Shockley W & Read W T, *Phys Rev*, 87 (5) (1952) 835.
28 Kung P-K, Li M-H, Lin C-F & Chen P, *J Mater Chem C*, 12 (29) (2024) 11181.
29 Suldozi R & Razaghi M, *Sci Rep*, 16 (2026) 19710.